Connection between sea surface anomalies and atmospheric quasi-stationary waves

Article

Accepted Version

Wolf, G., Czaja, A., Brayshaw, D. J. and Klingaman, N. P. (2020) Connection between sea surface anomalies and atmospheric quasi-stationary waves. Journal of Climate, 33 (1). pp. 201-212. ISSN 1520-0442 doi: https://doi.org/10.1175/JCLI-D-18-0751.1 Available at https://centaur.reading.ac.uk/85868/

To link to this article DOI: http://dx.doi.org/10.1175/JCLI-D-18-0751.1

Publisher: American Meteorological Society

Connection between sea surface anomalies and atmospheric quasi-stationary waves

G. Wolf*

Department of Meteorology, University of Reading, Reading, United Kingdom.

National Centre for Atmospheric Sciences, University of Reading, Reading, United Kingdom

A. Czaja

Imperial College, London, United Kingdom

D.J. Brayshaw and N.P. Klingaman

Department of Meteorology, University of Reading, Reading, United Kingdom.

National Centre for Atmospheric Sciences, University of Reading, Reading, United Kingdom

**Corresponding author address:* G. Wolf, Department of Meteorology, Earley Gate, University of Reading, P.O. Box 243, Reading, Berkshire RG6 6BB, United Kingdom.

E-mail: g.a.wolf@reading.ac.uk

ABSTRACT

Large scale, quasi-stationary atmospheric waves (QSWs) are known to be strongly connected with extreme events and general weather conditions. Yet, despite their importance, there is still a lack of understanding about what drives variability in QSW. This study is a step towards this goal, and identifies three statistically significant connections between QSWs and sea surface anomalies (temperature and ice cover) by applying a maximum covariance analysis technique to reanalysis data (1979-2015). The two most dominant connections are linked to the El Niño Southern Oscillation and the North Atlantic Oscillation. They confirm the expected relationship between QSWs and anomalous surface conditions in the tropical Pacific and the North Atlantic, but they cannot be used to infer a driving mechanism or predictability from the sea surface temperature or the sea ice cover to the QSW. The third connection, in contrast, occurs between late winter to early spring Atlantic sea ice concentrations and anomalous QSW patterns in the following late summer to early autumn. This new finding offers a pathway for possible long term predictability of late summer QSW occurrence.

1. Introduction

Weather in mid-latitudes is typically associated with synoptic scale transient cyclones and anti-cyclones, but occasionally more persistent weather regimes on scales of several days to about two weeks can be observed (Horel 1985). These persistent weather regimes are often associated with blocking highs at the jet exit regions (Masato et al. 2014) as part of a longitudinally extended "quasi-stationary" wave (QSW, e.g. Nakamura et al. 1997; Wolf et al. 2018b).

QSWs are important because of their strong influence on weather and their link to extreme events. Periods with increased QSW activity tend to be associated with more extremes, whereas the absence of QSWs is linked to "near-average" weather (Screen and Simmonds 2014; Wolf et al. 2018b). This connection between extreme events and mid-latitude wave patterns has been suggested in several case studies (e.g. Petoukhov et al. 2016; Fragkoulidis et al. 2018) although it is difficult to infer a general relationship from case studies alone (Screen and Simmonds 2013; Petoukhov et al. 2013). Wolf et al. (2018b) showed the most dominant Northern Hemisphere QSW patterns and the QSW patterns most relevant for European temperature extremes and anomalies events and temperature anomalies, with strong correlations also to seasonal averages.

Despite the importance of QSWs, there is still a lack of understanding about possible large scale drivers of the QSW variability. Most promising is the strong suggestion from literature that large-scale low-frequency variability patterns, like El Niño Southern Oscillation (ENSO) or North Atlantic Oscillation (NAO), can be linked to QSW patterns. Further, sea surface temperature (SST) and sea ice concentration (SIC) anomalies seem to be linked to jet variability and therefore also to QSW patterns.

ENSO may control the spatial and temporal variability of QSW activity of a full season, leading to extreme events in North America (Trenberth and Guillemot 1996; Pan et al. 1999). It is well known that a tropical heating source can lead to stationary anomalies in the general circulation (Gill 1980), but its effects on non-stationary waves in mid-latitudes and teleconnections to extreme events are less clear. Souders et al. (2014) have shown the anomalous wave pattern occurrence for transient waves during La Niña and El Niño. Furthermore, the impact of ENSO on the Atlantic is weaker and modulated by the Atlantic multidecadal oscillation, such that during its negative phase the ENSO teleconnection is more apparent (Rodríguez-Fonseca et al. 2016).

In Europe, the NAO has a strong influence on temperature anomalies (Pozo-Vázquez et al. 2001) and even strong droughts can be associated with the NAO phase (López-Moreno and Vicente-Serrano 2008). To some extent, the NAO can be related to processes outside the Atlantic region, connected by the presence of a wave. Jiang et al. (2017) showed that the Madden-Julian Oscillation influences the behavior and persistence of NAO positive and negative phases. Feldstein (2003) investigated the time evolution of the NAO associated with transients and QSWs, showing a connection between the positive NAO and a preceding Pacific wavetrain.

The connection between sea ice anomalies and circulation changes are of particular importance, because the persistence of sea ice anomalies makes them a possible source of seasonal to inter-annual predictability. There is progress in understanding the connection between a changing climate and the tropospheric and stratospheric circulation response (e.g. review of Screen et al. 2018), but the impact of sea ice on mid-latitude waves in a changing climate is still uncertain and widely discussed. Some studies conclude that stronger sea ice loss leads to decreased baroclinicity which can lead to more persistent wave patterns (e.g. Overland et al. 2016), whereas other studies link reduced sea ice with fewer planetary waves due to a weakening of the baroclinic-eddy wave source (e.g. Smith et al. 2017). These discrepancies highlight the necessity to further investigate and understand the atmospheric wave response to variability in sea surface temperatures and sea ice. It is difficult to isolate the atmospheric response to changes in sea ice due to the many other influences on the atmospheric circulation, as well as a low signal-to-noise-ratio (Screen et al. 2014). Regarding this aspect, Luo et al. (2019) highlighted the importance of the weakened north-south gradient of background potential vorticity (PV) over Eurasia for Ural blocking and cold winters in East Asia. The weakened PV gradient was linked therein to a warming climate and reduced sea ice. The cold events, however, can also occur during a weakened PV gradient even without negative sea ice anomalies as a result of mid-latitude cold anomalies, but still only if there is blocking. Such dependencies could be responsible for some of the above-mentioned discrepancies and the difficulties to come to a clear conclusion.

Several studies link specific local changes in sea ice to impacts on the atmospheric circulation. Wu et al. (2013) showed that above average winter sea ice concentrations west of Greenland can lead to Atlantic SST anomalies persisting into spring, which feed back on the atmospheric summer circulation in northern Eurasia. Hall et al. (2017) showed that the Atlantic May SST tripole, showing increased correlations with SST anomalies of the preceding months, can be associated with the Atlantic jet speed in summer, while sea ice anomalies could also be related to a latitudinal shift in the jet location. Petrie et al. (2015) found the Labrador sea ice concentration to be relevant for the jet strength over North America, which affects north-western Europe via downstream developing wave packets. Cause and effect between QSWs and sea ice anomalies is not always obvious and should be considered with caution (Simmonds and Govekar 2014). For example, Sato et al. (2014) linked anomalous sea ice retreats in the Barents-Kara sea to a shift in the Gulf Stream front, leading to an atmospheric wave response with a teleconnection to the Arctic. These studies further motivate investigating the connection between sea ice anomalies and QSW patterns.

The remainder of this paper is organized as follows. Section 2 presents the data and methods used to calculate QSWs and to relate them to surface ocean anomalies (sea surface temperature and sea ice concentrations). Results obtained by the application of the statistical method described in section 2 are presented in section 3. Section 4 analyses the connection between late winter/early spring sea surface anomalies and the associated QSW patterns in late summer/early autumn and its possible physical connections. The key conclusions of this paper are summarized in section 5.

2. Data and methods

ERA-Interim reanalysis (Dee et al. 2011) is used for all meteorological quantities on a longitude-latitude grid with $0.75^\circ \times 0.75^\circ$ resolution. The data are linearly detrended at each gridpoint over 1979 to 2015 for each season individually. This procedure allows us to focus on the intra-annual connections between variables, without the effect of long term trends.

To identify the envelope field of the quasi-stationary waves (QSW) at 300 hPa we use the method of Wolf et al. (2018b). The envelope field of the QSW is a phase independent, non-negative measure of the waviness of the anomalous meridional wind, v', in the zonal direction. We refer to this envelope field as the amplitude of the QSW. The anomalous meridional wind is calculated as $v' = \tilde{v} - \overline{\tilde{v}}$, where $\tilde{v}$ is the 15-day lowpass filtered meridional wind - to remove faster transients - and $\overline{\tilde{v}}$ is the daily climatology, to which we also applied a 15 day lowpass filter.

From this anomalous wind field, the phase-independent amplitude of the wave is calculated using the method of Zimin et al. (2003). For this method a wavenumber range must be chosen, which is assumed to represent the spatial scale of the waves of interest. In this study a wavenumber range of about 4 to 8 in mid-latitudes is chosen, but instead of using a fixed wavenumber range, a latitude-dependent wavenumber range is used, with a cosine decay towards higher latitudes, following the maxima of the power spectra of the anomalous meridional wind v' (Wolf et al. 2018b, details therein)[1]. The cosine weighting essentially leads to a latitude-independence of the

[1]The data for the 12 hourly envelope fields of the quasi-stationary waves between 1 June 1979 and 31 August 2015, are available at the Centre for Environmental Data Analysis (Wolf et al. 2018a).

range of wavelengths, rather than of the wavenumbers. An advantage of the applied QSW method, compared to other commonly used methods (such as Screen and Simmonds 2014; Kornhuber et al. 2017), is that it is a positive and phase independent measure of the wave packet in longitude-latitude fields for one time-step. This allows to represent the spatial pattern of the investigated wave packets and the application of time averages without having to deal with the problems of phase cancellation (as it would be the case for time averages of anomalies of geopotential height or meridional wind).

To identify statistical connections between QSWs and SST and SIC we apply a maximum co-variance (MC) analysis between those variables, as described in Czaja and Frankignoul (2002). The MC is calculated between monthly averaged anomaly fields. The anomalies are calculated as the deviation from the climatological mean of the specific month. The regions used for the MC analysis of the two variables are not necessarily the same and will be defined later. This method identifies the modes that maximize the covariance between two possibly different variables, similar to empirical orthogonal functions, which identify the modes that maximize the variance of one variable in the underlying data. For investigating the covariance between different seasons, monthly anomalies within each season are used. The term "season" refers to a period of any three consecutive months. Introducing further a time lag for one of the variables identifies potentially causal relationships. To give similar weight to each season, the anomalies are further normalized by the standard deviation of the specific variables in the specific season. To identify the relevance of specific modes, a Monte Carlo approach is applied to determine if the modes are statistically significant. The method is therefore a purely statistical approach to connect variables in the underlying data; it does not include any information about the nature of possible physical connections. For the MC analysis of two variables in different seasons, the Monte Carlo approach repeats the MC calculation 1000 times (if not stated otherwise) by holding the first variable fixed, but randomly permutating the years for the second variable. The permutation is, however, only applied to each season as a whole. This means that consecutive months within one season in the MC analysis are preserved in the Monte Carlo approach; only the years are shuffled. It is important to realize that the results of the MC analysis cannot by themselves be used as proof of causality, even when strong lead/lag relationships are found between variables. Instead, MCA analysis is used here to identify potential causal patterns in order to stimulate the further investigations required to identify physical causal processes.

To represent sea surface anomalies, we combine the fields of SST and SIC into one matrix, before applying the MC analysis. To do so, both fields are normalized by their seasonal standard deviation, using all gridpoints at which anomalies could be observed in the dataset for the associated season. For SIC, this includes all gridpoints inside the maximum areal extent of SIC in the dataset. The combined matrix is created by concatenating both normalized matrices along the latitude dimension. The MC analysis then proceeds as usual by assuming that the combined field represents one variable. In the following, we will refer to the combined field as SSTSIC. The MC patterns using either SST or SIC individually are qualitatively very similar. In case of a difference to the combined SSTSIC, this will be highlighted in the text. Note that the technique is linear so that the signs of patterns shown in the figures below can be reversed (the relative signs between QSW and SSTSIC remaining unchanged).

The values for the global pattern indices used in this study, namely the North Atlantic Oscillation (NAO) and the El Niño Southern Oscillation in the Niño 3.4 region (Niño 3.4), are retrieved from the CPC database of the National Oceanic and Atmospheric Administration (http://www.cpc.ncep.noaa.gov).

3. Connection between ocean anomalies and QSWs

In this section we identify connections between anomalous QSW amplitudes and anomalies in SSTSIC using monthly averages. We do this by applying the MC analysis between those two variables, as described in section 2, for various regions and with lags between -6 and $+9$ months (QSW leads surface variables at negative lags). Results are shown in Fig. 1a (extended Northern Hemisphere SSTSIC anomalies) and Fig. 2a (Atlantic SSTSIC anomalies). These figures display in colour the squared covariance of the leading MC mode between QSW and SSTSIC as a function of season and time lag, following Czaja and Frankignoul (2002, their Fig. 1). For example in Fig. 1a, large squared covariances are found when SSTSIC is taken in NDJ (x-axis) and QSW two months later (JFM, white rectangle highlighted). It is worth noting that the largest synchronous values occur during the colder seasons. Statistical significance is indicated by the green plusses in these plots while the contours display the correlation coefficient between large scale modes of climate variability and the QSW leading mode timeseries. Application of this procedure reveals three statistically significant connections which are discussed in the following three subsections.

a. Connection between QSWs and El Niño Southern Oscillation

High covariances for the first MC mode between extended Northern Hemisphere SSTSIC (20°S to 85°N) and extratropical Northern Hemisphere QSWs (30°N to 85°N) in Fig. 1a identify strong lead/lag connections between those variables for all seasons. The connection for all seasons can be understood by a persistent SSTSIC anomaly from the warmer seasons into the colder seasons (strong covariances along the diagonal line from top left to bottom right in Fig. 1a) with strong QSW anomalies manifestating only during the colder seasons. Due to the persistence of these increased covariances, the covariances during summer with large positive lags are also potentially physically meaningful, although not statistically significant. Since the statistically significant covariances (green dots and plusses) occur in an area of the plot which does show high correlations between the time series of the principal component of QSW and the Niño 3.4 index (black contours in Fig. 1a), we can associate this connection to El Niño Southern Oscillation (ENSO). Since this connection represents the clear first mode in the MC analysis, ENSO can be identified, on a hemispheric scale, as the dominant oceanic anomaly associated with QSW variability.

The diagonal tilting of the statistically significant covariances in Fig. 1a along a straight line indicates that this connection exists for QSW patterns mainly from DJF to FMA. Due to the connection to ENSO with the strongest anomalies in the tropical Pacific, it is not surprising that this specific connection is dominated by the SST contribution and cannot be reproduced by using SIC only (not shown).

The associated latitude-longitude pattern of the MC mode between SSTSIC in NDJ and QSW amplitudes in JFM (lag of $+2$ months, white box in Fig. 1a) shows increased QSW amplitudes over the Pacific, North America and the subtropical Atlantic and decreased QSW amplitudes over Europe and the high-latitude North Atlantic during La Niña (Fig. 1b, continuous and dashed contours, respectively - the La Niña state is clearly seen in the SST anomaly pattern shown in colour in Fig. 1b). Due to the linearity of the MC analysis, the exact opposite is true for El Niño (flipped signs for both SSTSIC and QSW). The patterns for the statistically significant covariances at positive lags are very similar, whereas for negative lags this is less clear (not shown here). Due to the long persistence of SST anomalies during ENSO phases of either sign and the statistical significance occurring at both positive and negative lags, it is impossible to deduce a direct forcing of QSW variability by the SST pattern in Fig. 1. Modeling work is necessary to understand how such strong covariances come about, perhaps through an atmospheric bridge (Lau and Nath 1994; Alexander et al. 2002). The connection between the ENSO SST pattern and QSW therefore suggests predictive skill for the QSW insofar as the ENSO SST pattern in itself tends to be strongly persistent (thus a month with warm SSTs tends to be followed by another warm SST month, consistent with similar QSW patterns being observed in both). This should not, however, be taken to imply a direct causal connection between ENSO SSTs and remote QSW anomalies at some later time. A seasonal forecast model that skillfully predicted the persistence for ENSO might also skillfully predict the preferred QSW pattern, but such an investigation is outside the scope of this paper.

b. Connection between QSWs and North Atlantic Oscillation

Using again the same region for the QSW amplitudes (30°N to 85°N), but reducing the region for the SSTSIC to the North Atlantic north of 20°N (80°W to 40°E), the first MC mode shows strong covariances associated with negative lags (Fig. 2a, i.e. QSW leads SSTSIC). These covariances are associated with the NAO (blue contour lines). The statistically significant covariances at negative lags suggest that the NAO-related SSTSIC pattern is reflecting a forcing of the ocean by the atmosphere, consistent with previous studies (e.g. Czaja and Frankignoul 2002; Visbeck et al. 2003). For the phase shown in Fig.2b, it consists of a tripolar SST anomaly, with colder conditions along the separated Gulf Stream sandwiched between anomalously warm conditions to the north and south (colours). The SIC pattern is, in response to a negative NAO phase, less sea ice in the Labrador sea (green contours) and more sea ice in the Greenland-Barents Sea (magenta contours).

The associated wave pattern (Fig. 2b, based on the lags/month highlighted by white box at negative lags in Fig. 2a) represents a reduction of wave amplitude over 30°N and an enhancement poleward of 50°N. It was shown to be associated with cold temperatures at 850 hPa in Central Europe (Wolf et al. 2018b), agreeing with previous results for temperature anomalies associated with the negative phase of the NAO (Pozo-Vázquez et al. 2001). The shift between the strongest covariances and highest correlation in Fig. 2a is the result of an evolving QSW pattern, from mid-latitudes towards high latitudes and a further shift from the Pacific towards the Atlantic (not shown here). Only the pattern at the later stage of this evolving QSW signal (Fig. 2b) is strongly correlated with the NAO, which is the reason for the reduced correlations occurring for the preceding seasons. However, the associated SST pattern is consistent and shows for all negative lags the typical NAO-like Atlantic SST-tripole (as the one in Fig. 2b) and therefore are those QSW patterns also expected to be associated with the NAO. As for the connection to ENSO, this connection is also associated dominantly with QSW anomalies during winter and the adjacent months. In winter, ENSO and NAO show strong correlations with the first three EOFs of Northern hemispheric QSW amplitudes (Wolf et al. 2018b), which highlights again the importance of these two QSW patterns.

c. Connection between QSWs and North Atlantic high latitude surface ocean anomalies

Besides the dominant two connections with ENSO or the NAO, we identified a third significant connection through MC analysis between late winter to early spring SSTSIC and late summer to early autumn QSW amplitudes (second white box in Fig. 2a, i.e. SSTSIC in FMA leads QSW by about 5 months).

The associated latitude-longitude QSW pattern in JAS shows increased mid-latitude and decreased high latitude QSW amplitudes (Fig. 2c), covarying with the SST tripole and SIC anomalies described above. That is, we find a very similar SSTSIC pattern but associated at lag $+5$ months with a generally opposing QSW pattern than found at lag -1 month (i.e., the signs of the anomaly in the high and mid-latitude regions are reversed). Note that the lags of $+4$ and $+6$ months show a consistent QSW pattern (not shown). In addition, the same statistically significant pattern can be reproduced using only SST or only SIC for the MC analysis, instead of the combined SSTSIC field (not shown here).

The pattern of increased mid-latitude QSW amplitudes in summer (Fig. 2c) is linked to strong lower troposphere temperature anomalies of either sign (but mainly warm anomalies) over Central Europe (Wolf et al. 2018b). QSW composites associated with extreme warm anomalies in the same region showed a very similar wave pattern. Further, cold anomalies in Central Europe were associated with preceding increased high latitude QSW activity. This suggests that the QSW patterns, related to European temperature anomalies in summer could be linked to Atlantic SSTSIC anomalies in late winter to early spring.

A further separation of the SSTSIC region into northern and southern parts (20°N to 60°N and 60°N to 85°N) reveals that the MC analysis for the northern part leads to statistically significant covariances, whereas MC analysis for the southern part does not (not shown here; see section 4 below for more sensitivity tests of the MC analysis). The associated longitude-latitude patterns for the northern part are very similar to the ones using the full Atlantic region (20°N to 85°N). This suggests the importance of high latitude sea surface anomalies for this connection, but the associated longitude-latitude patterns for the southern part show similarities to the ones for the northern part, at least for lags of +5 and +6 months, meaning that the southern part is not necessarily irrelevant for this teleconnection. The role of the SIC in this connection is investigated further in section 4.

To check the robustness of this connection between FMA SSTSIC and subsequent JAS QSW amplitudes, we calculated composite FMA SSTSIC anomalies for the 8 JAS seasons with the strongest QSW anomalies in mid- (225°W to 45°E, 40°N to 60°N: 1987, 1985, 1998, 1981, 2003, 2007, 1986 and 1995) and high latitudes (North of 65°N: 1984, 1995, 1993, 1979, 2008, 1991, 1983 and 2004), where the years given in brackets are ordered by their intensity, starting with the highest intensity. The resulting SSTSIC patterns are very similar to the one given in Fig. 2c (not shown). The results are not sensitive to the number of seasons used for the composite. This supports the hypothesis of a connection between SSTSIC in FMA and QSW amplitudes in the following JAS. We now briefly investigate possible physical mechanisms for this connection.

4. Possible physical links for the inter-seasonal ocean and QSW connection

In the previous section we have already shown the importance of the high-latitude Atlantic for the connection between late winter/early spring SSTSIC anomalies and late summer/early autumn QSW amplitude anomalies. Using only SIC for the MC analysis leads to more statistically significant signals of the same patterns for neighbouring seasons with similar lags (Fig. S1), additional to the previously found statistically significant signal at a lag of $+5$ months for FMA by using SST only or SSTSIC (Fig. 2a). From this we can hypothesize that SIC is the main contributor to this connection. Such SIC anomalies, if persistent enough, could interact with the large scale atmospheric circulation by modifying the baroclinicity, acting on similar sub-annual timescales as in previous studies (e.g. Wu et al. 2013). We possibly see an atmospheric response in summer and not spring, because of the importance of the jet location relative to the region of the modified baroclinicity. The center (defined by the peak intensity) of the lower tropospheric jet at 850 hPa in the Atlantic jet entry region may still be too far south in April to June (climatological value at 42°N, between 60°W and 30°W), whereas in July to September it shifts northward (climatological value at 49°N). This means that the change in baroclinicity by the higher-latitude ocean anomalies close to the Labrador Sea in April to June do not align well with the jet position in the West Atlantic, which therefore does not optimally contribute as a baroclinic energy source for further wave amplification. This could change, once the climatological jet location moves towards higher latitudes in the following months. As discussed in the introduction, this source of energy could be a relevant mechanism for wave amplification (e.g. Smith et al. 2017). How this interaction works clearly needs further investigation but the statistical result reported here appears robust. We proceed below to further analysis of the empirical relationship captured in Fig. 2c.

To interact with the late summer atmospheric circulation, the late winter SIC anomalies must be persistent enough. To check the persistence of these SIC anomalies, we calculate a lag composite of area-averaged SST and SIC anomalies in the Greenland-Barents Sea (0°E to 60°E, 50°N to 80°N) and Labrador Sea (70°W to 50°W, 50°N to 65°N) for the 8 seasons with the strongest positive and negative SIC differences between those two regions in FMA (Fig. 3a). As a reminder, those regions are chosen to cover the relevant SIC anomalies for the investigated connection in this section (see Fig. 2b and c). We refer to this difference as I_{diff}. Positive values indicate more anomalous sea ice in the Greenland-Barents Sea than in the Labrador Sea. All composite anomalies (SST and SIC) for positive I_{diff} (solid lines) and negative I_{diff} (dashed lines) show the same sign until JAS. This persistence is insensitive to the number of seasons used for the composite. If these anomalies are optimally aligned to interact with the wave guide in summer, this could cause the anomalous QSW patterns in summer.

Similar to the previous test of robustness, we calculate the QSW patterns in JAS for the years with the strongest positive (1979, 2011, 2010, 1981, 1998, 1987, 2004 and 2003) and negative values (1984, 1993, 1983, 1990, 1992, 1991, 1995 and 2014) for I_{diff}. As expected from the results of the MC analysis, the composite for the years with negative I_{diff} values leads to anomalously strong high latitude QSW amplitudes (Fig. 3b), exceeding the 99th percentile (white dots). The composite for the years with positive I_{diff} values leads to anomalous strong and statistically significant mid-latitude QSW amplitudes (Fig. 3c), although there is a gap of increased QSW amplitudes over North America. But overall, the sign of I_{diff} clearly leads to a separation of the QSW patterns with strong values at high or mid-latitudes. The qualitative results are insensitive to the exact choice of the regions used to calculate I_{diff}, as long as they capture the dipole character of this anomaly.

Comparing the SSTSIC in Fig. 2b and 2c reveals very similar patterns. This suggests that the NAO, which is strongly associated with the QSW and SST pattern of Fig. 2b, represents the common feature behind both connections (the ones shown in Fig. 2b and Fig. 2c). The associated SSTSIC pattern found for both connections therefore appears to link the two atmospheric anomalies in autumn/winter and the following summer/autumn. This would mean that the autumn/winter QSW pattern leads to a specific late winter/spring SSTSCI pattern which further leads to a specific QSW pattern in late summer/early autumn. In the following we will provide further support for this hypothesis. First for the connection between winter NAO index and the following late summer/early autumn QSW anomalies. For this connection we obtain a linear correlation of -0.42 between mid-latitude (225°W to 45°E and 40°N to 60°N) averaged QSW amplitudes in JAS and the averaged NAO value in the preceding DJF (Fig. S2a), whereas strong high-latitude (north of 65°N) averaged QSW amplitudes in JAS seem to occur mainly after a positive NAO in the preceding DJF (Fig. S2b). Second, if the above hypothesis is true, one can possibly expect increased covariances between similar QSW patterns in autumn/winter and the following summer/autumn. To test this we repeated the MC analysis of Fig. 2a between extratropical Northern Hemisphere QSW amplitudes and QSW amplitudes limited to the Atlantic basin (instead of SSTSIC limited to the Atlantic basin). The QSW amplitudes in the second region are restricted to the Atlantic basin, because of the known strong connection between Atlantic QSW anomalies and the NAO (Wolf et al. 2018b, or Fig. 2a and 2b herein). This MC analysis indeed shows a statistically significant connection between autumn to winter Atlantic QSW amplitudes and Northern Hemisphere QSW amplitudes with about a $+7$ month lag, which further show increased correlations with NAO (Fig. S3). Because of the strong atmospheric internal variability and its nonlinear behaviour, the presented linear statistical method does not prove this hypothesis, but supports the potential for recurrent interactions between QSWs, SST and SIC anomalies between autumn to winter and late summer to early autumn. To clarify the details of these recurrent interactions, further analysis is necessary.

5. Conclusion and discussion

In a previous study (Wolf et al. 2018b) we showed the connection between QSWs and European weather and extreme events and identified the main modes of QSW variability. We highlighted therein the importance of better understanding the physical mechanisms underlying these QSW patterns and their variability. This analysis represents the first step towards this goal by investigating the link between surface ocean anomalies and QSW amplitudes with lags of several months. Therefore, we use the MC analysis as a powerful tool to identify statistical connections between different variables, as done in previous studies (e.g. Czaja and Frankignoul 2002; Frankignoul et al. 2014).

We identified three statistical significant connections between sea surface anomalies and anomalous QSW amplitudes. The two most dominant connections occur during the colder seasons (late autumn, winter, early spring) and can be related to ENSO and NAO. These global pattern indices are not only linked to strong temperature anomalies and extreme events (e.g. Pan et al. 1999; Pozo-Vázquez et al. 2001; López-Moreno and Vicente-Serrano 2008), but they can also be associated with some predictability (Latif et al. 1998; Scaife et al. 2014). It is therefore important to understand the evolution of the associated QSW patterns, which are more directly linked to the associated weather and therefore can help to get a deeper understanding of the evolution of extremes or why predictability increases in remote regions. This is no contradiction with the previous statement that our results for the ENSO connection cannot be used to infer predictability for the QSWs. The results from the applied statistical method could only be used to highlight the general connection between the SST associated with ENSO and mid-latitude QSWs. The QSW pattern itself indicates possible teleconnection regions, but to understand the details of the teleconnections or the time evolution and frequency of the QSWs during an ENSO event, further analysis beyond this monthly lagged analysis is needed. During La Niña we identified an increase in QSW amplitudes over the North Pacific and North America, reaching downstream into the subtropical Atlantic towards the Mediterranean, whereas over the high-latitude North Atlantic and Europe a decrease in QSW amplitudes can be observed. For the Atlantic SST tripole, associated with the negative NAO phase, QSW amplitudes show increased values at high latitudes with a maximum over the Atlantic and a slight decrease along the subtropical Asian jet. This connection exists for QSW amplitudes with negative lags in the MC analysis, suggesting the SST tripole to be an imprint of the preceding atmospheric flow pattern. This dominant atmosphere-driving-ocean relationship is in agreement with previous studies (e.g. Czaja and Frankignoul 2002; Visbeck et al. 2003). These QSW patterns, associated with NAO and ENSO, explain a large contribution of the overall QSW variability during the cold season. The focus in that paragraph, concerning the global pattern indices, was towards La Niña and the negative NAO phase. Due to the linearity of the MC analysis, the exact opposite is true for El Niño or the positive NAO (reversed signs for both SSTSIC and QSW, relative signs remain unchanged).

The third statistical significant connection between those two variables occurs between FMA Atlantic high latitude sea surface anomalies and JAS extratropical Northern Hemisphere QSW anomalies. We identified the SIC as the main contributor to this connection. The large lag of about +5 months can possibly be attributed to the persistence of the associated SIC pattern. We showed that for years with a strong anomaly of such a SIC pattern in FMA, this anomaly persists into JAS. Interacting with the general circulation, these sea ice anomalies could be responsible for the QSW response in the following late summer/early autumn. The reason why this interaction is not apparent during late spring/early summer could be that the locations between the baroclinic modified region by the SIC or associated SST anomalies and the wave guide for the QSWs are not optimally aligned. How this interaction works in detail needs further investigation.

Our results about the FMA SSTSIC anomalies show strong similarities with the findings of Frankignoul et al. (2014), in which they showed that the Atlantic SIC anomalies in the Labrador sea and Greenland-Barents Sea (they refer to it as “seesaw” pattern) during late winter/early spring can be associated to preceding NAO anomalies and which by itself leads to a NAO-like pattern of opposite polarity about 6 weeks later. This suggests the same underlying driving mechanism between winter NAO and FMA SSTSIC anomalies, but distinct to the analysis of Frankignoul et al. (2014), we identified a longer lag connection between their “seesaw” pattern and upper tropospheric QSWs in JAS. In agreement with our findings, they also identified SIC anomalies as the main contributor to this connection. They further discussed that including the North Pacific SIC dipole pattern of negative and positive anomalies in the Bering and Okhotsk Sea, which appears also in our findings (see Fig. 2c), increases the statistical significance.

To test the robustness of the results, we included a composite analysis, showing the same sea surface or QSW patterns as for the linear MC analysis by applying a ± 5 months lag to each of the composited variables separately. This further increases the confidence in the findings of the applied statistical analysis. Due to the findings of the connection between NAO and QSW anomalies in autumn to winter, the connection between winter NAO and FMA SSTSIC anomalies and the connection between FMA SSTSIC anomalies and JAS QSW anomalies, we hypothesized that a connection between autumn to winter QSWs and QSWs in the following JAS may be apparent. Repeating the MC analysis for QSW amplitudes between different seasons does indeed show increased covariances, supporting this hypothesis.

These results are all based on the first MC modes for the different regions or variables, to highlight the most dominant and robust signals. Higher MC modes also include some statistically significant signals, but those are fewer and less coherent. The second MC modes show mainly two statistically significant signals. For SSTSIC in the extratropical Northern Hemisphere (first mode given in Fig. 1a) the area of the statistically significant covariances is very similar to the one found for negative lags in Fig. 2a, also with increased correlations with the winter NAO index, meaning that the second MC mode for extratropical Northern Hemisphere SSTSIC describes the same signal as the first MC mode for SSTSIC in the Atlantic region. The second MC mode for SSTSIC in the Atlantic shows statistically significant signals in spring to summer, with a lag of about +4 months. The SSTSIC signal is represented again by the previously discussed NAO-like imprint. The associated QSW patterns are also partly very similar to the signal found for FMA with a +5 lag, suggesting that the previously identified SSTSIC not only appears in late winter, but also into spring and summer. The patterns are less coherent, however, and besides the very similar QSW pattern we can also identify a similar SSTSIC pattern, but which is associated with a east-west dipole in QSW amplitudes, with positive anomalies towards Europe and negative over North America for a negative NAO. This second mode could explain the gap of increased mid-latitude QSW amplitudes in the composite study (Fig. 3c).

In this paper we were able to link some important QSW patterns to surface ocean anomalies. Due to the more direct link of the QSW patterns to the associated weather, compared to the use of global pattern indices, their consideration can be helpful in the understanding and interpretation of specific teleconnection patterns. We further demonstrated the relevance of SIC anomalies on the QSW patterns of following seasons, which can be very helpful for long term predictability of large scale weather conditions or the occurrence of extremes.

Acknowledgments. We acknowledge funding from the Natural Environment Research Council (NERC) for the ODYSEA project (grant number: NE/M006085/1). Nicholas P. Klingaman was funded by a NERC Independent Research Fellowship (NE/L010976/1).

References

Alexander, M. A., I. Blad, M. Newman, J. R. Lanzante, N.-C. Lau, and J. D. Scott, 2002: The atmospheric bridge: The influence of enso teleconnections on airsea interaction over the global oceans. *Journal of Climate*, **15 (16)**, 2205–2231, doi:10.1175/1520-0442(2002)015⟨2205:TABTIO⟩2.0.CO;2.

Czaja, A., and C. Frankignoul, 2002: Observed impact of atlantic sst anomalies on the north atlantic oscillation. *J. Climate*, **15 (6)**, 606–623, doi:10.1175/1520-0442(2002)015⟨0606:OIOASA⟩2.0.CO;2.

Dee, D. P., and Coauthors, 2011: The era-interim reanalysis: configuration and performance of the data assimilation system. *Quart. J. Roy. Meteor. Soc.*, **137 (656, A)**, 553–597, doi:10.1002/qj.828.

Feldstein, S. B., 2003: The dynamics of nao teleconnection pattern growth and decay. *Quart. J. Roy. Meteor. Soc.*, **129 (589)**, 901–924, doi:10.1256/qj.02.76.

Fragkoulidis, G., V. Wirth, P. Bossmann, and A. H. Fink, 2018: Linking northern hemisphere temperature extremes to rossby wave packets. *Quart. J. Roy. Meteor. Soc.*, **144 (711)**, 553–566, doi:10.1002/qj.3228.

Frankignoul, C., N. Sennéchael, and P. Cauchy, 2014: Observed atmospheric response to cold season sea ice variability in the arctic. *J. Climate*, **27 (3)**, 1243–1254, doi:10.1175/JCLI-D-13-00189.1.

Gill, A. E., 1980: Some simple solutions for heatinduced tropical circulation. *Quart. J. Roy. Meteor. Soc.*, **106 (449)**, 447–462, doi:10.1002/qj.49710644905.

Hall, R. J., J. M. Jones, E. Hanna, A. A. Scaife, and R. Erdélyi, 2017: Drivers and potential predictability of summer time north atlantic polar front jet variability. *Climate Dyn.*, **48 (11)**, 3869–3887, doi:10.1007/s00382-016-3307-0.

Horel, J. D., 1985: Persistence of the 500 mb height field during northern hemisphere winter. *Mon. Wea. Rev.*, **113 (11)**, 2030–2042, doi:10.1175/1520-0493(1985)113⟨2030:POTMHF⟩2.0.CO;2.

Jiang, Z., S. B. Feldstein, and S. Lee, 2017: The relationship between the maddenjulian oscillation and the north atlantic oscillation. *Quart. J. Roy. Meteor. Soc.*, **143 (702)**, 240–250, doi:10.1002/qj.2917.

Kornhuber, K., V. Petoukhov, D. Karoly, S. Petri, S. Rahmstorf, and D. Coumou, 2017: Summertime planetary wave resonance in the northern and southern hemispheres. *J. Climate*, **30 (16)**, 6133–6150, doi:10.1175/JCLI-D-16-0703.1.

Latif, M., and Coauthors, 1998: A review of the predictability and prediction of enso. *Journal of Geophysical Research: Oceans*, **103 (C7)**, 14 375–14 393, doi:10.1029/97JC03413.

Lau, N.-C., and M. J. Nath, 1994: A modeling study of the relative roles of tropical and extratropical sst anomalies in the variability of the global atmosphere-ocean system. *Journal of Climate*, **7 (8)**, 1184–1207, doi:10.1175/1520-0442(1994)007⟨1184:AMSOTR⟩2.0.CO;2.

López-Moreno, J. I., and S. M. Vicente-Serrano, 2008: Positive and negative phases of the wintertime north atlantic oscillation and drought occurrence over europe: A multitemporal-scale approach. *J. Climate*, **21 (6)**, 1220–1243, doi:10.1175/2007JCLI1739.1.

Luo, D., X. Chen, J. Overland, I. Simmonds, Y. Wu, and P. Zhang, 2019: Weakened potential vorticity barrier linked to recent winter arctic sea ice loss and midlatitude cold extremes. *Journal of Climate*, **32 (14)**, 4235–4261, doi:10.1175/JCLI-D-18-0449.1.

Masato, G., T. Woollings, and B. J. Hoskins, 2014: Structure and impact of atmospheric blocking over the euro-atlantic region in present-day and future simulations. *Geophys. Res. Lett.*, **41 (3)**, 1051–1058, doi:10.1002/2013GL058570.

Nakamura, H., M. Nakamura, and J. Anderson, 1997: The role of high- and low-frequency dynamics in blocking formation. *Mon. Wea. Rev.*, **125 (9)**, 2074–2093, doi:10.1175/1520-0493(1997)125⟨2074:TROHAL⟩2.0.CO;2.

North, G., T. Bell, R. Cahalan, and F. Moeng, 1982: Sampling errors in the estimation of empirical orthogonal functions. *Mon. Wea. Rev.*, **110 (7)**, 699–706, doi:10.1175/1520-0493(1982)110⟨0699:SEITEO⟩2.0.CO;2.

Overland, J., and Coauthors, 2016: Nonlinear response of mid-latitude weather to the changing arctic. *Nature Climate Change*, **6**, 992–999, doi:10.1038/NCLIMATE3121.

Pan, Z., M. Segal, R. Arritt, T. Chen, and S. Weng, 1999: A method for simulating effects of quasi-stationary wave anomalies on regional climate. *J. Climate*, **12 (5, 1)**, 1336–1343, doi:10.1175/1520-0442(1999)012⟨1336:AMFSEO⟩2.0.CO;2.

Petoukhov, V., S. Petri, S. Rahmstorf, D. Coumou, K. Kornhuber, and H. J. Schellnhuber, 2016: Role of quasiresonant planetary wave dynamics in recent boreal spring-to-autumn extreme events. *Proc. Natl. Acad. Sci. (USA)*, **113 (25)**, 6862–6867, doi:10.1073/pnas.1606300113.

Petoukhov, V., S. Rahmstorf, S. Petri, and H. J. Schellnhuber, 2013: Reply to screen and simmonds: From means to mechanisms. *Proceedings of the National Academy of Sciences*, **110 (26)**, E2328–E2328, doi:10.1073/pnas.1305595110.

Petrie, R. E., L. C. Shaffrey, and R. T. Sutton, 2015: Atmospheric response in summer linked to recent arctic sea ice loss. *Quart. J. Roy. Meteor. Soc.*, **141 (691)**, 2070–2076, doi:10.1002/qj.2502.

Pozo-Vázquez, D., M. J. Esteban-Parra, F. S. Rodrigo, and Y. Castro-Díez, 2001: A study of nao variability and its possible non-linear influences on european surface temperature. *Climate Dyn.*, **17 (9)**, 701–715, doi:10.1007/s003820000137.

Rodríguez-Fonseca, B., and Coauthors, 2016: A review of enso influence on the north atlantic. a non-stationary signal. *Atmosphere*, **7 (7)**, doi:10.3390/atmos7070087.

Sato, K., J. Inoue, and M. Watanabe, 2014: Influence of the gulf stream on the barents sea ice retreat and eurasian coldness during early winter. *Environmental Research Letters*, **9 (8)**, 084 009, doi:10.1088/1748-9326/9/8/084009.

Scaife, A. A., and Coauthors, 2014: Skillful longrange prediction of european and north american winters. *Geophys. Res. Lett.*, **41 (7)**, 2514–2519, doi:10.1002/2014GL059637.

Screen, J. A., T. J. Bracegirdle, and I. Simmonds, 2018: Polar climate change as manifest in atmospheric circulation. *Current Climate Change Reports*, **4 (4)**, 383–395, doi:10.1007/s40641-018-0111-4.

Screen, J. A., C. Deser, I. Simmonds, and R. Tomas, 2014: Atmospheric impacts of arctic sea-ice loss, 1979–2009: separating forced change from atmospheric internal variability. *Climate Dynamics*, **43 (1)**, 333–344", doi:10.1007/s00382-013-1830-9.

Screen, J. A., and I. Simmonds, 2013: Caution needed when linking weather extremes to amplified planetary waves. *Proceedings of the National Academy of Sciences*, **110 (26)**, E2327–E2327, doi:10.1073/pnas.1304867110.

Screen, J. A., and I. Simmonds, 2014: Amplified mid-latitude planetary waves favour particular regional weather extremes. *Nature Climate Change*, **4 (8)**, 704–709, doi:10.1038/nclimate2271.

Simmonds, I., and P. D. Govekar, 2014: What are the physical links between arctic sea ice loss and eurasian winter climate? *Environmental Research Letters*, **9 (10)**, 101 003, doi:10.1088/1748-9326/9/10/101003.

Smith, D. M., N. J. Dunstone, A. A. Scaife, E. K. Fiedler, D. Copsey, and S. C. Hardiman, 2017: Atmospheric response to arctic and antarctic sea ice: The importance of oceanatmosphere coupling and the background state. *J. Climate*, **30 (12)**, 4547–4565, doi:10.1175/JCLI-D-16-0564.1.

Souders, M. B., B. A. Colle, and E. K. M. Chang, 2014: The climatology and characteristics of rossby wave packets using a feature-based tracking technique. *Mon. Wea. Rev.*, **142 (10)**, 3528–3548, doi:10.1175/MWR-D-13-00371.1.

Trenberth, K., and C. Guillemot, 1996: Physical processes involved in the 1988 drought and 1993 floods in north america. *J. Climate*, **9 (6)**, 1288–1298, doi:10.1175/1520-0442(1996)009⟨1288:PPIITD⟩2.0.CO;2.

Visbeck, M., E. P. Chassignet, R. G. Curry, T. L. Delworth, R. R. Dickson, and G. Krahmann, 2003: *The Ocean's Response to North Atlantic Oscillation Variability*, 113–145. American Geophysical Union (AGU), doi:10.1029/134GM06.

Wolf, G., D. J. Brayshaw, N. P. Klingaman, and A. Czaja, 2018a: Envelope field of northern hemispheric upper tropospheric (300 hpa) quasi-stationary waves (june 1979 to august 2015). *Centre for Environmental Data Analysis*, doi:10.5285/c0c7998800414e46b6823dc75751bb4c.

Wolf, G., D. J. Brayshaw, N. P. Klingaman, and A. Czaja, 2018b: Quasi-stationary waves and their impact on european weather and extreme events. *Quart. J. Roy. Meteor. Soc.*, **144 (717)**, 2431–2448, doi:10.1002/qj.3310.

Wu, B., R. Zhang, R. D'Arrigo, and J. Su, 2013: On the relationship between winter sea ice and summer atmospheric circulation over eurasia. *J. Climate*, **26 (15)**, 5523–5536, doi:10.1175/JCLI-D-12-00524.1.

Zimin, A. V., I. Szunyogh, D. Patil, B. R. Hunt, and E. Ott, 2003: Extracting envelopes of rossby wave packets. *Mon. Wea. Rev.*, **131 (5)**, 1011–1017, doi:10.1175/1520-0493(2003)131⟨1011:EEORWP⟩2.0.CO;2.

6. Figures

LIST OF FIGURES

Fig. 1. **Panel (a)** shows the first MC mode for the lagged covariance matrix between extended Northern Hemisphere (20°S to 85°N) SSTSIC and extratropical Northern Hemisphere (30°N to 85°N) QSW anomalies. Shading represents covariance between associated anomalies, weighted by their respective seasonal standard deviation. Seasons for the SSTSIC fields are given in panel (a) on the x-axis and are represented by the initial letters of the associated months. For the seasonally averaged QSW amplitudes a lag of -6 to $+9$ months is applied (given on the y-axis); positive lags therefore mean that the SSTSIC is leading QSW. Green plusses (dots) show statistical significant covariances based on 95th (90th) percentile. Red dots show those instances when the MC mode is not separable from the following mode, following the rule of thumb of North et al. (1982). Additional contour lines represent correlations between one of two global pattern indices (Niño 3.4 in black and NAO in blue) and the lagged QSW MC mode.
Panel (b) shows the associated latitude-longitude pattern for the box, marked by the white edges in panel (a), for NDJ SSTSIC and JFM QSW (lag of $+2$ months). Boundaries for the regions used in the MC analysis are given by the black dashed lines. Shading shows anomalies of SST. Gray solid (dashed) contour lines show positive (negative) anomalies of QSW amplitude, spaced every $0.5\,\mathrm{m/s}$ omitting the zero contour line. Magenta (positive values) and green (negative values) contour lines show anomalies in SIC, spaced every 0.04 omitting the zero contour line. All variables shown are calculated via the projection of this variable onto the timeseries of the first principal component. 28

Fig. 2. First MC mode between Atlantic (80°W to 50°E and 20°N to 85°N) SSTSIC and extratropical Northern Hemisphere (30°N to 85°N) lagged QSW anomalies (boundaries of these regions shown by black dashed lines in panel (b) and (c)). Panel (b) and (c) show the associated latitude-longitude pattern for the boxes, marked by the white edges in panel (a), for JFM SSTSIC and DJF QSW (panel b, lag -1 month) and for FMA SSTSIC and JAS QSW (panel c, lag $+5$ months). Gray solid (dashed) contour lines show positive (negative) anomalies of QSW amplitude, spaced every $0.25\,\mathrm{m/s}$ omitting the zero contour line. Description for all other shadings, contours, etc. are the same as in Fig. 1. 29

Fig. 3. Panel a shows SST and SIC persistence for a composite of the 8 years with the strongest positive and negative I_{diff} values in FMA. I_{diff} represents the difference of SIC box averages between the Labrador Sea (70°W to 50°W, 50°N to 65°N) and Greenland-Barents Sea (0°E to 60°E, 50°N to 80°N). Blue and black lines show the averaged values of SST and SIC in the Greenland-Barents Sea; red and magenta lines show the averaged values of SSTSIC in the Labrador Sea. Values associated with positive (negative) values of I_{diff} are given by solid (dashed) lines. All values are seasonally detrended and normalized by the associated seasonal standard deviation. Panel b (panel c) shows the associated anomalous QSW amplitudes in JAS for the same composite years with $I_{\text{diff}} < 0$ ($I_{\text{diff}} > 0$). Statistical significance above the 95th (99th) percentile is given by the green (white) dots. Mean QSW amplitudes are given by the contour lines, spaced every 0.75 m/s, starting at 7.5 m/s. 30

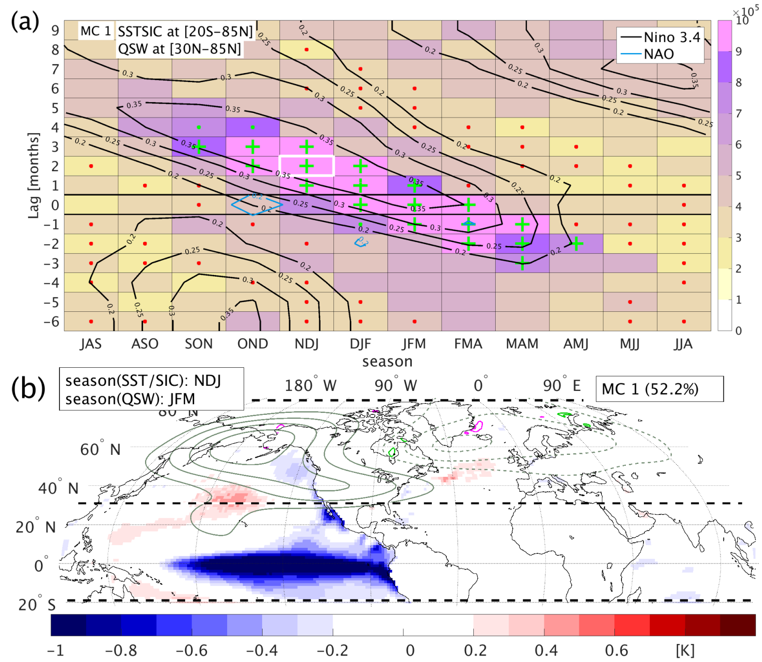

FIG. 1. **Panel (a)** shows the first MC mode for the lagged covariance matrix between extended Northern Hemisphere (20°S to 85°N) SSTSIC and extratropical Northern Hemisphere (30°N to 85°N) QSW anomalies. Shading represents covariance between associated anomalies, weighted by their respective seasonal standard deviation. Seasons for the SSTSIC fields are given in panel (a) on the x-axis and are represented by the initial letters of the associated months. For the seasonally averaged QSW amplitudes a lag of -6 to $+9$ months is applied (given on the y-axis); positive lags therefore mean that the SSTSIC is leading QSW. Green plusses (dots) show statistical significant covariances based on 95th (90th) percentile. Red dots show those instances when the MC mode is not separable from the following mode, following the rule of thumb of North et al. (1982). Additional contour lines represent correlations between one of two global pattern indices (Niño 3.4 in black and NAO in blue) and the lagged QSW MC mode.

Panel (b) shows the associated latitude-longitude pattern for the box, marked by the white edges in panel (a), for NDJ SSTSIC and JFM QSW (lag of $+2$ months). Boundaries for the regions used in the MC analysis are given by the black dashed lines. Shading shows anomalies of SST. Gray solid (dashed) contour lines show positive (negative) anomalies of QSW amplitude, spaced every $0.5\,\mathrm{m/s}$ omitting the zero contour line. Magenta (positive values) and green (negative values) contour lines show anomalies in SIC, spaced every 0.04 omitting the zero contour line. All variables shown are calculated via the projection of this variable onto the timeseries of the first principal component.

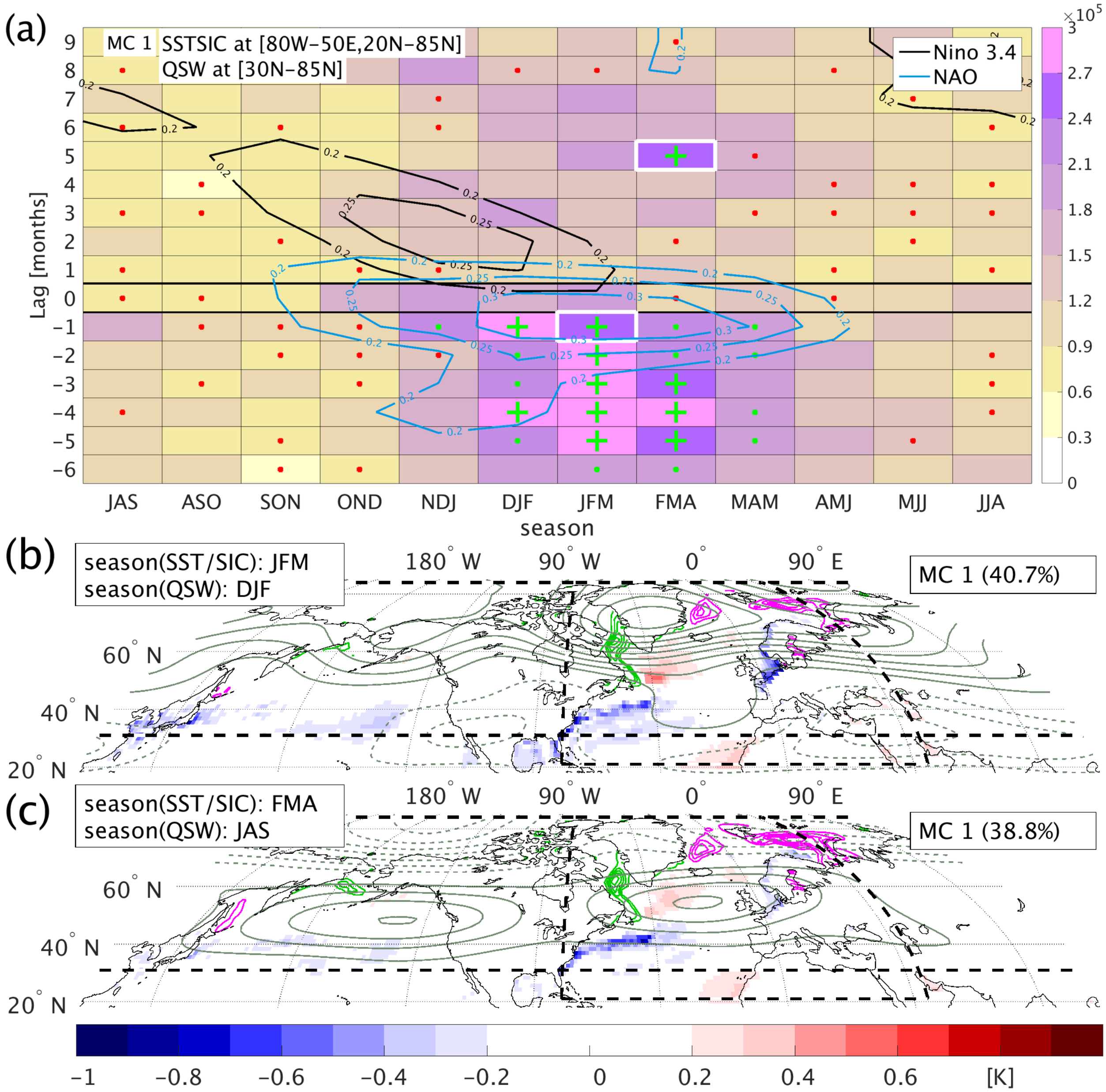

FIG. 2. First MC mode between Atlantic (80°W to 50°E and 20°N to 85°N) SSTSIC and extratropical Northern Hemisphere (30°N to 85°N) lagged QSW anomalies (boundaries of these regions shown by black dashed lines in panel (b) and (c)). Panel (b) and (c) show the associated latitude-longitude pattern for the boxes, marked by the white edges in panel (a), for JFM SSTSIC and DJF QSW (panel b, lag −1 month) and for FMA SSTSIC and JAS QSW (panel c, lag +5 months). Gray solid (dashed) contour lines show positive (negative) anomalies of QSW amplitude, spaced every 0.25 m/s omitting the zero contour line. Description for all other shadings, contours, etc. are the same as in Fig. 1.

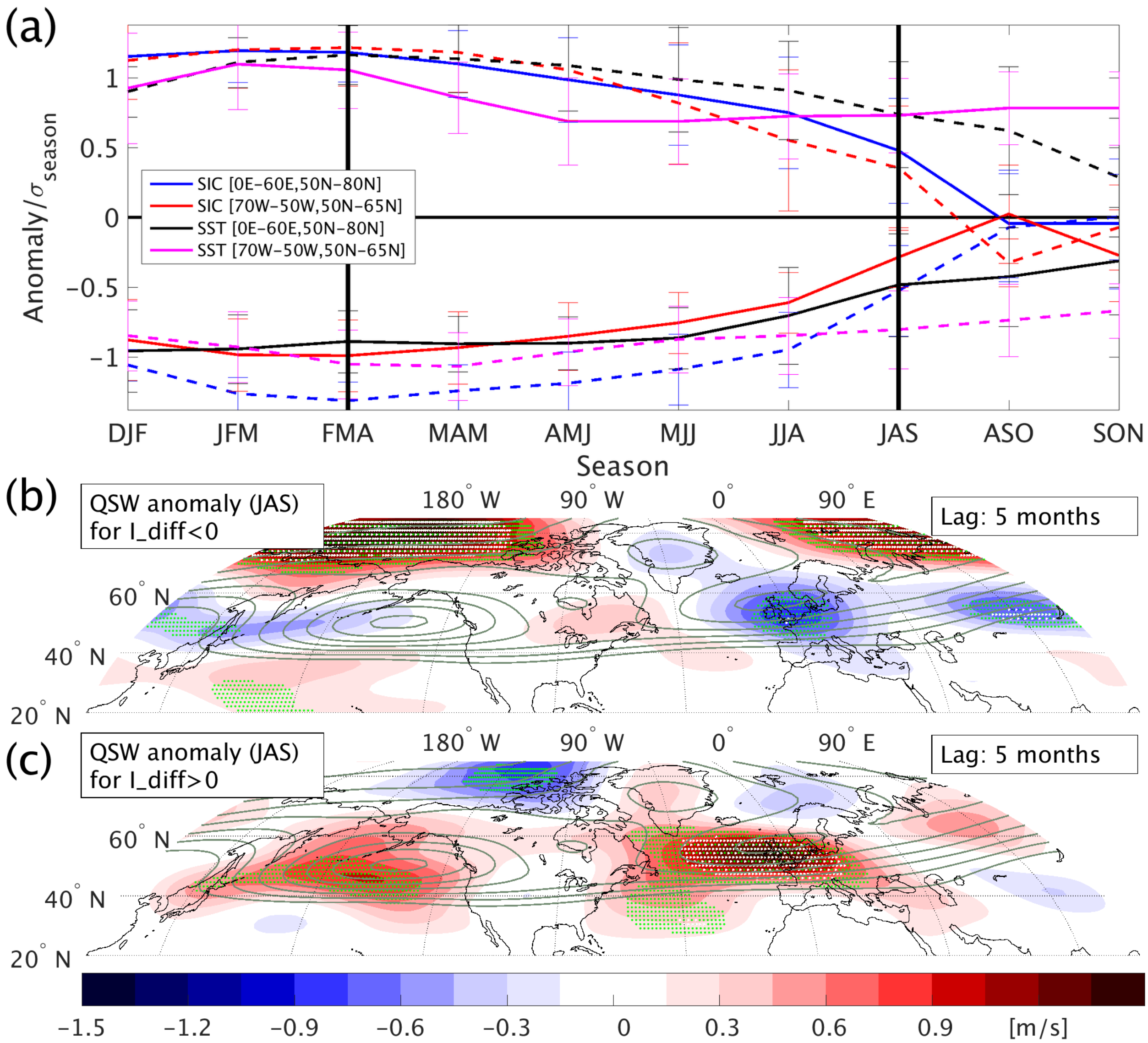

FIG. 3. Panel a shows SST and SIC persistence for a composite of the 8 years with the strongest positive and negative I_{diff} values in FMA. I_{diff} represents the difference of SIC box averages between the Labrador Sea (70°W to 50°W, 50°N to 65°N) and Greenland-Barents Sea (0°E to 60°E, 50°N to 80°N). Blue and black lines show the averaged values of SST and SIC in the Greenland-Barents Sea; red and magenta lines show the averaged values of SSTSIC in the Labrador Sea. Values associated with positive (negative) values of I_{diff} are given by solid (dashed) lines. All values are seasonally detrended and normalized by the associated seasonal standard deviation. Panel b (panel c) shows the associated anomalous QSW amplitudes in JAS for the same composite years with $I_{\text{diff}} < 0$ ($I_{\text{diff}} > 0$). Statistical significance above the 95th (99th) percentile is given by the green (white) dots. Mean QSW amplitudes are given by the contour lines, spaced every 0.75 m/s, starting at 7.5 m/s.